

Terahertz shaping technology based on coherent beam combining

Xiao-Ran Zheng(郑晓冉), Dan-Ni Ma(马丹妮), Guang-Tong Jiang(蒋广通), Cun-Lin Zhang(张存林), and Liang-Liang Zhang(张亮亮)

Citation: Chin. Phys. B, 2023, 32 (**11**): 114210. DOI: 10.1088/1674-1056/acc2b0

Journal homepage: http://cpb.iphy.ac.cn; http://iopscience.iop.org/cpb

What follows is a list of articles you may be interested in

High efficiency of broadband transmissive metasurface terahertz polarization converter

Qiangguo Zhou(周强国), Yang Li(李洋), Yongzhen Li(李永振), Niangjuan Yao(姚娘娟), and Zhiming Huang(黄志明)

Chin. Phys. B, 2023, 32 (**2**): 024201. DOI: 10.1088/1674-1056/ac6db7

Multi-function terahertz wave manipulation utilizing Fourier convolution operation metasurface

Min Zhong(仲敏) and Jiu-Sheng Li(李九生)

Chin. Phys. B, 2022, 31 (**5**): 054207. DOI: 10.1088/1674-1056/ac46c0

Creation of multi-frequency terahertz waves by optimized cascaded difference frequency generation

Zhong-Yang Li(李忠洋), Jia Zhao(赵佳), Sheng Yuan(袁胜), Bin-Zhe Jiao(焦彬哲), Pi-Bin Bing(邴丕彬), Hong-Tao Zhang(张红涛), Zhi-Liang Chen(陈治良), Lian Tan(谭联), and Jian-Quan Yao(姚建铨)

Chin. Phys. B, 2022, 31 (**4**): 044205. DOI: 10.1088/1674-1056/ac29b4

High-sensitive terahertz detection by parametric up-conversion using nanosecond pulsed laser

Yuye Wang(王与烨), Gang Nie(聂港), Changhao Hu(胡常灏), Kai Chen(陈锴), Chao Yan(闫超), Bin Wu(吴斌), Junfeng Zhu(朱军峰), Degang Xu(徐德刚), and Jianquan Yao(姚建铨)

Chin. Phys. B, 2022, 31 (**2**): 024204. DOI: 10.1088/1674-1056/ac2d20

Coherent beam combination of adaptive fiber laser array with tilt-tip and phase-locking control

Wang Xiong (王雄), Wang Xiao-Lin (王小林), Zhou Pu (周朴), Su Rong-Tao (粟荣涛), Geng Chao (耿超), Li Xin-Yang (李新阳), Xu Xiao-Jun (许晓军), Shu Bo-Hong (舒柏宏)

Chin. Phys. B, 2013, 22 (**2**): 024206. DOI: 10.1088/1674-1056/22/2/024206

Terahertz shaping technology based on coherent beam combining

Xiao-Ran Zheng(郑晓冉)[1], Dan-Ni Ma(马丹妮)[2], Guang-Tong Jiang(蒋广通)[3,†], Cun-Lin Zhang(张存林)[1], and Liang-Liang Zhang(张亮亮)[1,‡]

[1] *Key Laboratory of Terahertz Optoelectronics, Ministry of Education, Beijing Key Laboratory for Terahertz Spectroscopy and Imaging, and Beijing Advanced Innovation Center for Imaging Technology, Department of Physics, Capital Normal University, Beijing* 100048, *China*

[2] *Beijing Key Laboratory for Precision Optoelectronic Measurement Instrument and Technology, School of Optics and Photonics, Beijing Institute of Technology, Beijing* 100081, *China*

[3] *Laser Industries Research Academy-Beijing, Hubei Huazhong Changjiang Photoelectric Science and Technology Ltd, Beijing* 102209, *China*

(Received 30 December 2022; revised manuscript received 4 March 2023; accepted manuscript online 9 March 2023)

The generation of terahertz (THz) waves by focusing a femtosecond pulsed laser beam at a distance is able to overcome the strong absorption properties of air and has rapidly attracted the attention of industry. However, the poor directionality of the THz wave radiation generated by this method is not conducive to THz wave applications. By controlling the morphology of the ultrafast laser-excited plasma filament and its electron density distribution through coherent beam combining technology, we achieve direct THz beam shaping and are able to obtain THz wave radiation of Gaussian or arbitrary transverse distribution. The novel experimental approach proposed in this paper opens up the research field of direct THz wave shaping using plasma. Moreover, it innovates multi-parameter convergence algorithms and, by doing so, has the potential to find beam patterns with higher energy conversion efficiency and break the energy limit of THz waves emitted by lasers at high power.

Keywords: femtosecond pulsed laser, coherent beam combining, terahertz wave, beam shaping, plasma

PACS: 42.25.Bs, 42.25.Kb, 52.38.–r, 87.50.U– **DOI:** 10.1088/1674-1056/acc2b0

1. Introduction

Terahertz (THz) waves generally refer to electromagnetic waves with a frequency of 0.1–10 THz (1 THz = 10^{12} Hz), situated between microwaves and infrared waves in the electromagnetic spectrum. The pulse width of a femtosecond pulse laser beam is between a few and hundreds of femtoseconds. It has ultra-short time characteristics and can generate high peak power. Femtosecond laser pulses with high pulse energy (pulse energy greater than a few hundred mJ) interact with gas atoms to excite free ions and electrons, creating a plasma. The plasma then rapidly decays while producing THz waves in a manner known as the 'air method'. As this method has the advantages of being able to generate THz waves with high peak power and a wide spectrum at long distance (several kilometers away), it is very promising for applications and has attracted a lot of attention from industry in recent years. However, the generation of THz waves using laser energy in this way is still relatively inefficient, and the mechanism of THz generation has not been fully explained. Thus, it is urgent to find ways to improve the energy conversion efficiency of THz waves. Researchers in this field have made many fruitful attempts to enhance the efficiency of THz generation by using two-color fields,[1,2] changing the focal length of the focusing lens,[3] changing the wavelength of the laser[4] and the working medium,[5] and adding electric field bias,[6] etc.

Recently, we have noticed some reports on the study of THz generation by special beams[7,8] and have carried out related studies. A Gaussian laser is shaped by a spatial light modulator or phase plates. By controlling the air plasma excited by ultrashort laser pulses, the enhancement of THz conversion efficiency and modulation of THz intensity distribution have finally been achieved. In 2022, Zhelin Zhang *et al.* used Bessel beams to generate THz radiation with a Bessel distribution.[8] These works have demonstrated that the THz intensity distribution can be effectively controlled by modulating the air plasma, which has the potential to achieve THz shaping. However, these reports do not propose a controllable shaping method to effectively seek the best laser mode. The complex physical phenomena within the excited air plasma after the focusing of each type of special beam cannot be accurately predicted, and we must rely on many experiments to find verification and blindly search for a more suitable type of special beam. Moreover, when using spatial light modulators or phase plates to change the focal field to modulate THz waves, the beam modulation devices cannot withstand the high power, limiting the use and development of the system.

In this paper, a THz generation method based on laser coherent beam combining (CBC) is proposed for the first time. Instead of a spatial light modulator or a phase plate, combining the air plasma-based THz source with CBC technology[9–12] to shape the laser beam can overcome the limitation of the SLM threshold on laser power. The beam locator and phase

†Corresponding author. E-mail: jgtop@qq.com
‡Corresponding author. E-mail: zhlliang@126.com

© 2023 Chinese Physical Society and IOP Publishing Ltd

shifter control the direction and phase of the laser beam in each channel, and thus control the plasma filament morphology and electron density distribution of the ultrafast excitation laser. Finally, the shaping of THz waves is achieved.

This article will focus on methods to achieve THz shaping using new techniques and will discuss the improvement of energy conversion efficiency from laser to THz waves. We use a THz camera for real-time acquisition of THz intensity and distribution. By adjusting the beam direction and phase of each channel, the traction control of the intensity distribution of THz waves towards the target is completed, and the shaping of THz waves is achieved. We use the convergence strategy of stochastic parallel gradient descent (SPGD) to achieve closed-loop regulation of the system. This method not only ignores the complex physical processes such as the actual density distribution inside the plasma, but also overcomes the dynamic perturbations of the system. The convergence process does not require an understanding of the specific electron density distribution inside the air plasma, and does not need clarification of all the physical principles, such as the coherence strategy between the beams. It can still use the evaluation function to control the convergence, which eventually realizes the regulation of THz wave and completes THz beam shaping. We can also use this method to find beam patterns with stronger energy conversion efficiency by adjusting the evaluation function.

Traditionally, THz beam shaping has been performed using spiral phase plates,[13] holographic diffraction gratings,[14] antenna arrays[15,16] and metamaterials,[17] but these methods are generally cumbersome, inefficient and difficult to prepare. Compared with conventional THz beam shaping techniques, the new technique performs THz beam shaping directly via plasma modulation, without energy loss and damage threshold limitation on laser power, and achieves programmable beam shaping by iterative algorithms.

This method can also be applied to THz modulation, since the laser field of the focused femtosecond pulsed laser beam correlates and corresponds to the optical field properties of THz waves.[8,18] The intensity, distribution, divergence angle or polarization characteristics of THz waves tend to be fixed under specific optical field conditions. Therefore, by reproducing a specific focal field, THz waves of a certain property can be generated. The modulation of THz waves is achieved indirectly through modulation of the laser field.

2. Optical path design

The first report of CBC was for continuous light waves;[19] it was then gradually extended to the field of pulses, with experiments related to nanosecond and femtosecond pulses[20,21] and successful shaping of beams from femtosecond pulses.[22] These studies have demonstrated that there are no longer any technical obstacles to the technique in experimental terms. In order to give the reader a clearer understanding of the technique, we provide an example of an experimental optical path.

In order to achieve the purpose of shaping the combining beam, the array beam first needs to meet the basic conditions of CBC, as follows. Each beam should have the same intensity, wavelength and polarization direction and a constant phase difference. The delay difference among these is zero while the phase difference is constant. Moreover, the phase and beam direction can be continuously controlled in a certain range, and an ultrashort laser should meet the requirements of generating THz waves. By controlling the beam phase and beam direction of the array, the synthetic light field is controlled. The electron density distribution of the air plasma excited by the ultrashort laser pulse is indirectly controlled to achieve the control of the THz intensity distribution. On this basis, it was investigated whether higher THz conversion efficiency could be obtained.

To meet these requirements, we designed an optical path for THz generation based on CBC technology, as shown in Fig. 1. We separated the optical path into five parts: laser CBC module, laser field detection module, THz generation module, THz detection module and computerized numerical control (CNC) terminal.

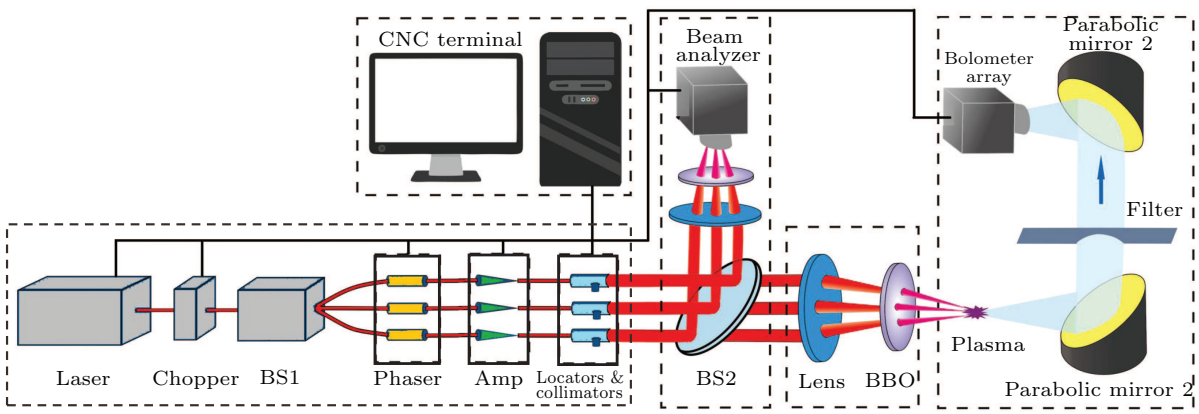


Fig. 1. Schematic diagram of the optical path for THz wave generation based on CBC technology.

The laser CBC module includes a seed laser, chopper, beam splitter (BS), phase shifter, master oscillator power amplifier (MOPA), beam locator and collimator. Among these, the seed laser uses a femtosecond pulse laser source to generate a seed beam with a pulse width of 50 fs, pulse repetition rate of 1 kHz and line width of 1 GHz. It also needs to ensure that the relevant parameters of the output Gaussian pulse laser after power amplification collimation remain unchanged. This module enables the control of multi-channel laser wavelength, power, deflection direction, chopping frequency, phase and other parameters, and completes the beam collimation emission. Through the THz generation module, the synthetic beam excites air plasma to generate THz waves. The intensity and distribution of the generated THz waves are detected by the THz detection module, and the state of the laser field under this THz intensity distribution is monitored by the laser field detection module. The purpose of the CNC terminal is to summarize the parameter information of the system, monitor the system status, realize the control of the parameters of the array laser and complete the closed-loop system.

We need to be aware that the laser power should meet the minimum requirements for ionizing air. The power density required to ionize air and produce a plasma filament depends on a variety of factors such as laser wavelength, pulse width and air pressure. In general, a power density of at least 1 GW·cm^{-2} is required at the focal point to ionize the air to form plasma and to satisfy the conditions for the generation of THz waves.

Theoretically this scheme is also applicable to monochromatic schemes; however, two-color laser schemes have been shown to achieve higher energy conversion efficiencies and have a rich theoretical basis,[1–3] so we have focused our research on two-color schemes. From the description of the transient photocurrent model,[18,23] we know that when the relative phase difference between the fundamental frequency and the second harmonic is $\pi/2$ the laser field is able to produce maximum symmetry breaking of the electron drift velocity, exciting the transient current and thus producing a THz wave. In experiments, the relative phases of the fundamental and second harmonics are usually controlled by adjusting the angle of laser incidence and the distance from the beta barium borate (BBO) crystal to the plasma. In general we need to adjust the position and angle of the BBO crystal to the actual situation in order to obtain maximum generation efficiency. Because the initial phase of each beam in this system is controlled, the relative phase combinations between the fundamental and second harmonics of the different beams are more flexible and variable, giving the opportunity to produce a greater degree of symmetry breaking and to obtain stronger THz waves.

For two-color field schemes, the profile of the second harmonic cannot be neglected. In general, the profiles of the fundamental frequency wave and the generated second harmonic are not exactly the same. This is because the profile of the second harmonic is influenced by various factors such as the propagation characteristics of the laser in the crystal, the profile of the incident laser field and the non-linear parameters of the crystal. The profile of the incident laser field is influenced by the laser input and the characteristics of the optical elements in the laser path, while the non-linear parameters of the crystal are influenced by the structure and chemical composition of the crystal. During second-harmonic generation, the direction and intensity of laser propagation in the crystal changes under the influence of non-linear optical effects, which affects the profile of the fundamental frequency and the second harmonic, resulting in a different distribution of the two beams. If two beams with the same profile are to be obtained, a high-precision optical system and a high-quality BBO crystal with precise control of the laser propagation in the crystal are required. In some cases, for example when using shorter laser path lengths (BBO crystal to plasma distance), the profile of the two beams generated may be identical.

3. Theoretical simulation

3.1. Theoretical basis for the generation of THz waves using CBC technology

The frequency and the polarization direction of each beam are the same, and they are all fundamental mode Gaussian beams. Assuming that the Gaussian beams of N bunches are arranged in a square array or hexagonal dense array in the emission plane at $z=0$, the center coordinates of the unit beam are (x_j, y_j) and the emission direction is along the z-axis. The light field distribution at the emission end (at the plane of $z=0$) can be written as

$$\begin{aligned} &E_0(x,y,z=0,\boldsymbol{\Phi}) \\ &= \sum_{j=1}^{N} A_j \exp\left[-\frac{(x-x_j)^2+(y-y_j)^2}{\omega_0^2}\right] \exp(\mathrm{i}\varphi_j) \\ &\quad \times \mathrm{circ}\left[\frac{\sqrt{(x-x_j)^2+(y-y_j)^2}}{d/2}\right]. \end{aligned} \tag{1}$$

Here, (x,y) is the coordinate system of the array element, A_j is the amplitude of the jth beam, ω_0 is the beam radius, φ_j is the initial phase of the jth beam at the emission plane, circ[ ] is the function of aperture and d is the aperture diameter of the jth beamlet. Also

$$\boldsymbol{\Phi} = [\varphi_1 - \varphi_1,\ \varphi_2 - \varphi_1,\ \varphi_3 - \varphi_1,\ \ldots,\ \varphi_N - \varphi_1]. \tag{2}$$

When the configuration and parameters of the beam array are determined, the relative phase vector decides the light field of the combined beam $\boldsymbol{\Phi}$. Under the near-axis approximation, the complex amplitude and intensity distribution of the combined beam at $z=L$ can be expressed as

$$E_{\mathrm{laser}}(u,v,z=L,\boldsymbol{\Phi})$$

$$= \frac{\exp\left[\frac{\mathrm{i}k}{2L}\left(u^2+v^2\right)\right]}{\mathrm{i}\lambda L} \times \mathcal{F}\left\{E_0\left(x,y,z=0;\Phi\right)\exp\left[\frac{\mathrm{i}k}{2}\left(\frac{1}{L}-\frac{1}{f}\right)\left(x^2+y^2\right)\right]\right\}, \tag{3}$$

$$I_{\text{laser}}\left(u,v,z=L,\Phi\right) = \left|E_{\text{laser}}\left(u,v,z=L;\Phi\right)\right|^2. \tag{4}$$

Here, (u,v) represents the coordinate of the laser CBC plane and λ, f, L and $\mathcal{F}\{\ \}$ represent the wavelength, focal length, propagation distance and Fourier transform, respectively.

The laser field excites the air plasma to produce THz radiation. We need to establish the relationship between the laser field and the THz radiation field. We refer to the model proposed by Kim *et al.*[18,24,25] and extrapolate backwards from the THz wavefield to the laser wavefield

$$\begin{aligned} &E_{\text{THz}}\left(p,q,\Omega\right) \\ &\propto k_{\text{THz}}\int_V A\left(u,v,z,\Omega\right)\sin\left[\theta\left(p,q,u,v,z\right)\right] \\ &\quad\times\exp\left(\mathrm{i}k_{\text{THz}}z\right)h\left(p,q,u,v,z,\Omega\right)\mathrm{d}u\mathrm{d}v, \end{aligned} \tag{5}$$

where (p,q) represents the coordinates of the THz receiving plane, Ω is the THz frequency and $A\left(u,v,z,\Omega\right)$ is the amplitude of the THz field generated at a point of the plasma at all frequencies. The amplitude of the THz center frequency is proportional to the square root of the plasma density, and varies between the points inside the plasma. The overall amplitude of the spectrum is also proportional to the plasma electron density N_{e}, and the time derivative of the electron density N_{e} can be expressed as $\mathrm{d}N_{\text{e}}/\mathrm{d}t \approx N_{\text{g}}w\left(t\right)$, where N_{g} is the neutral particle density and $w\left(t\right)$ is the ionization rate. Keldysh and Perelomov *et al.* proposed a formula for calculating the ionization rate of the gas optical field based on the laser wavelength and dielectric ionization potential,[26,27] where the ionization rate is proportional to the laser intensity $w\left(t\right) \propto \left|E_{\text{laser}}\right|^2$. $A \propto J = \int e\cdot v_{\text{e}}\left(t\right)N_{\text{e}}\left(t\right)\mathrm{d}t \propto \int eN_{\text{g}}w\left(t\right)v_{\text{e}}\left(t\right)\mathrm{d}t \propto \int eN_{\text{g}}\left|E_{\text{laser}}\right|^3\mathrm{d}t$. Here, J is the photocurrent, e is the electron charge, $v_{\text{e}}\left(t\right)$is the electron velocity and $v_{\text{e}}\left(t\right) \propto E_{\text{laser}}$.

The $\sin\left[\theta\left(u,v,z\right)\right]$ term describes the relative phase walk-off between the fundamental and second-harmonic waves during their propagation in the plasma, and the resulting modulation of the THz field amplitude. In the case of plasma refractive index inhomogeneity, this phase difference can be calculated as $\theta\left(u,v,z\right) = \theta_0 + \int_z \Delta n\left(u,v,z'\right)k_\omega\,\mathrm{d}z'$, where the refractive index difference Δn can be expressed as

$$\begin{aligned} \Delta n\left(u,v,z'\right) &= \left[n_{\text{air},\omega}\left(u,v,z'\right)+n_{\text{plasma},\omega}\left(u,v,z'\right)\right] \\ &\quad-\left[n_{\text{air},\omega}\left(u,v,z'\right)+n_{\text{plasma},2\omega}\left(u,v,z'\right)\right]. \end{aligned}$$

Here, the plasma refractive index is

$$n_{\text{plasma},\omega}\left(u,v,z'\right) = \sqrt{1-\omega_{\text{p}}^2(u,v,z')/\omega^2}.$$

The plasma frequency is

$$\omega_{\text{p}}^2\left(u,v,z'\right) = \sqrt{4\pi e^2 N_{\text{e}}(u,v,z')/m_{\text{e}}},$$

where m_{e} is the electron mass and ω is the laser frequency. $h\left(u,v,z,\Omega\right)$ represents the phase change obtained inside the plasma by the generated THz radiation. At any point in the ray trajectory between the source point and the receiving plane, if the THz frequency is less than the plasma frequency, the THz wave is blocked.

$$h\left(u,v,z,\Omega\right) = \begin{cases} 0, & \Omega < \omega_{\text{p}}, \\ \exp\left[\mathrm{i}\int_V k_{\text{THz}}\left[n_{\text{THz}}\left(u,v,z,\Omega\right)-1\right]\mathrm{d}u\mathrm{d}v\right], & \Omega \geq \omega_{\text{p}}, \end{cases}$$

where the THz refractive index is

$$n_{\text{THz}}\left(u,v,z,\Omega\right) = \frac{1}{\sqrt{1-\omega_{\text{p}}^2\left(u,v,z\right)/\Omega^2}}.$$

We can deduce the relationship between the THz distribution and the laser field distribution as

$$\begin{aligned} E_{\text{THz}} \propto k_{\text{THz}}\cdot e\cdot N_{\text{g}}\int_{\text{V}}\Bigg[\int\left|E_{\text{laser}}\right|^2\mathrm{d}t \\ \times\iint\left(E_{\text{laser},\omega}-E_{\text{laser},2\omega}\right)\mathrm{d}t\,\mathrm{d}z\exp\left(\mathrm{i}kz\right)\Bigg]\mathrm{d}u\mathrm{d}v, \end{aligned} \tag{6}$$

and

$$I_{\text{THz}} = \left|E_{\text{THz}}\right|^2. \tag{7}$$

We were surprised that Bessel beams could be used to generate THz waves that conform to the Bessel beam distribution.[8] Therefore, we have reason to believe that the phenomenon can be extended to complex laser field pumps to generate THz waves of any mode by plasma modulation. Also, higher laser-to-THz wave energy conversion efficiency was obtained by using a ring Airy beam,[7] and by the same token we believe that beam types with higher energy conversion efficiency can be found by modulation of complex laser fields by convergence algorithms. We simulate the THz distribution generated by Gaussian and Bessel beams by the same calculation. As shown in Fig. 2, the simulation results are basically consistent with the experimental results.[8,25]

There are four main physical processes involved from the laser source to the THz wave detection plane. Namely, the process of CBC of the array laser, the laser excitation of the plasma, the generation of THz waves by the plasma and the transmission of THz waves through the plasma and air to the receiving plane. Due to the transient nature of the two-color field plasma generation process, the complex non-linear effects and the influence of frequency doubling crystals on the second-harmonic profile, it is difficult to perform high-precision surface array measurements of high-temperature

plasma with existing measurement techniques, and even with numerical simulations the actual density distribution inside the plasma is still difficult to predict accurately. This is one of the difficulties in further investigating the physical mechanism of THz wave generation in plasma.

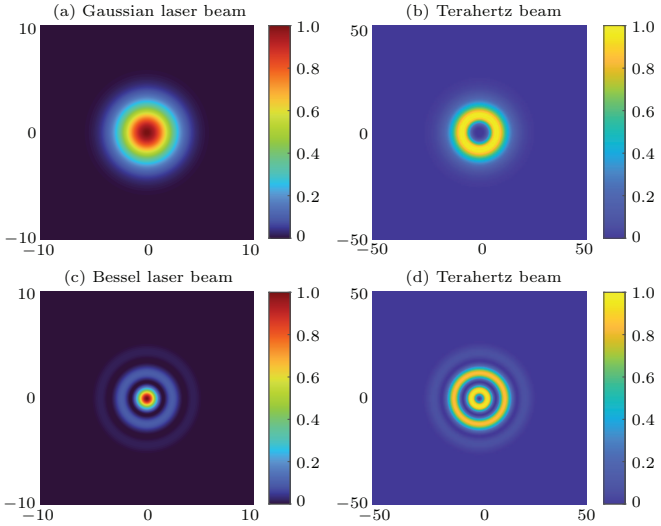


Fig. 2. Schematic diagram of laser field intensity distribution and THz intensity distribution. (a) Focal field light intensity distribution of a Gaussian-type laser. (b) Intensity distribution of the THz wave generated by the Gaussian-type laser. (c) Focal field light intensity distribution of a zero-order Bessel-type laser. (d) Intensity distribution of a THz wave generated by the zero-order Bessel-type laser.

These complex physical phenomena can be avoided by using the SPGD convergence algorithm, which is very similar to the 'black box process' in deep learning models, where the internal mechanism of the black box model is not transparent but can still be used to obtain the desired results through a large number of random perturbations. The user is only concerned with the inputs and outputs of the model, not with the internal mechanisms, and the evaluation function is set to guide the direction of convergence. The mapping relationship is calibrated by the two typical experimental phenomena described above and used to perform simulations. This simplified mapping relationship does not affect the logical process of convergence of the closed-loop system. In other words, the convergence method proposed in this paper can be applied even though the actual situation is more complex than the simulated one.

By setting the objective function, namely the ideal THz distribution function, the actual collected THz intensity distribution image is compared with the ideal distribution. The degree of similarity between them is used as the evaluation function of the convergence algorithm to guide the system to achieve convergence and complete THz shaping. By analyzing the convergence results, we can observe the optical axis of the array beam and the phase information, as well as the relationship between the intensity distribution of the laser focus field and that of the THz wave. It provides a new way to explore the plasma, which helps us to find more typical experimental phenomena and further analyze the physical mechanism of THz wave generation by plasma.

3.2. Evaluation functions and convergence strategies

In order to achieve the purpose of THz shaping, we use the two-dimensional correlation coefficient between the target matrix and the actual matrix as the evaluation function. The correlation coefficient between the measured value A and the target value B is calculated. The higher the correlation coefficient is, the closer the measured value is to the target value. When the correlation coefficient is 1, the measured values are exactly the same as the target value. The formula for calculating the two-dimensional correlation coefficient function is

$$J = \frac{\sum_m \sum_n (A_{mn} - A'')(B_{mn} - B'')}{\sqrt{\left(\sum_m \sum_n (A_{mn} - A'')^2\right)\left(\sum_m \sum_n (B_{mn} - B'')^2\right)}}. \quad (8)$$

For the convenience of demonstration, we multiply the two-dimensional correlation coefficient by 100% to describe the similarity.

We can take different evaluation methods for different needs, such as using the power in the bucket to find a stronger peak intensity of the THz wave, and obtaining a higher conversion efficiency from laser energy to THz energy.

The convergence strategy used in this paper is the SPGD algorithm, which is a fast and effective gradient evaluation method. By applying random perturbations to all control parameters in the performance evaluation function $J(U)$, the gradient estimation is completed according to the amount of change in the evaluation function after the perturbation.

For THz shaping systems based on CBC technology, the control signal output is an analog voltage signal. Three control parameters are involved in the iterative process, which are horizontal direction control parameters x, vertical direction control parameters y and phase control parameters p. The iterative formula of the SPGD algorithm can be expressed as

$$\begin{aligned} & U_j^{(n+1)}(v_x, v_y, v_p) \\ &= U_j^{(n)}(v_x, v_y, v_p) + r\delta J^{(n)} \delta U_j^{(n)}(v_x, v_y, v_p), \end{aligned} \quad (9)$$

where $U_j^{(n)}(v_x, v_y, v_p)$ is the control variable and (v_x, v_y, v_p) represent the horizontal direction control voltage, vertical direction control voltage, and phase control voltage, respectively: $v_x = [v_{x1}, v_{x2}, v_{x3}, \ldots, v_{xN}]$, $v_y = [v_{y1}, v_{y2}, v_{y3}, \ldots, v_{yN}]$, $v_p = [v_{p1}, v_{p2}, v_{p3}, \ldots, v_{pN}]$. r is the iterative step, $\delta J^{(n)}$ is the amount of change in the performance evaluation function before and after the perturbation, $J^{(n)}$ is the value of the system performance evaluation function before and after the perturbation and $\delta U_j^{(n)}$ is the statistically independent random perturbation.

When using the SPGD algorithm for control, the specific implementation processes are as follows:

1. Generate a pseudo-random code vector and convert it to a voltage signal δU, with random perturbations satisfying a mean of zero and equal variance.

2. Apply the random perturbation voltage δU to each driver to obtain the value of the evaluation function $J^+ = J(u+\delta U)$, and then apply a reverse perturbation voltage to obtain the evaluation function of the negative perturbation $J^- = J(u-\delta U)$.

3. Calculate the amount of change in the evaluation function $\delta J = J(U-\delta U)$.

4. Update the control parameters according to the formula $U_{\mathrm{j}}^{(n+1)} = U_j^{(n)} + r\delta J^{(n)}\delta U_j^{(n)}$.

5. Repeat steps 1–4.

3.3. Simulation calculation and analysis

According to the theories described above, the simulation model is established to explore the influence of beam array arrangement, the number of array beam, disturbance step length, parallel quantities and convergence strategy on THz shaping.

First, we tried two common structures, hexagonal dense and square arrays. As shown in Fig. 3(a), the hexagonal dense array structure has a higher duty cycle than the square array structure. Under the same convergence strategy, we compared three hexagonal dense arrays and square arrays with similar beam counts. As shown in Figs. 3(b) and 3(c), we find that the hexagonal dense arrays can achieve a faster and better convergence effect than the square arrays. We attribute this advantage to the superiority of the hexagonal dense array arrangement. The hexagonal dense array has a higher duty cycle and a better distribution because six beams are evenly distributed around each beam. Although the square beam has eight beams distributed around it, the distance between the middle beam and each side beam is not the same, and this difference leads to a significant difference in CBC results.

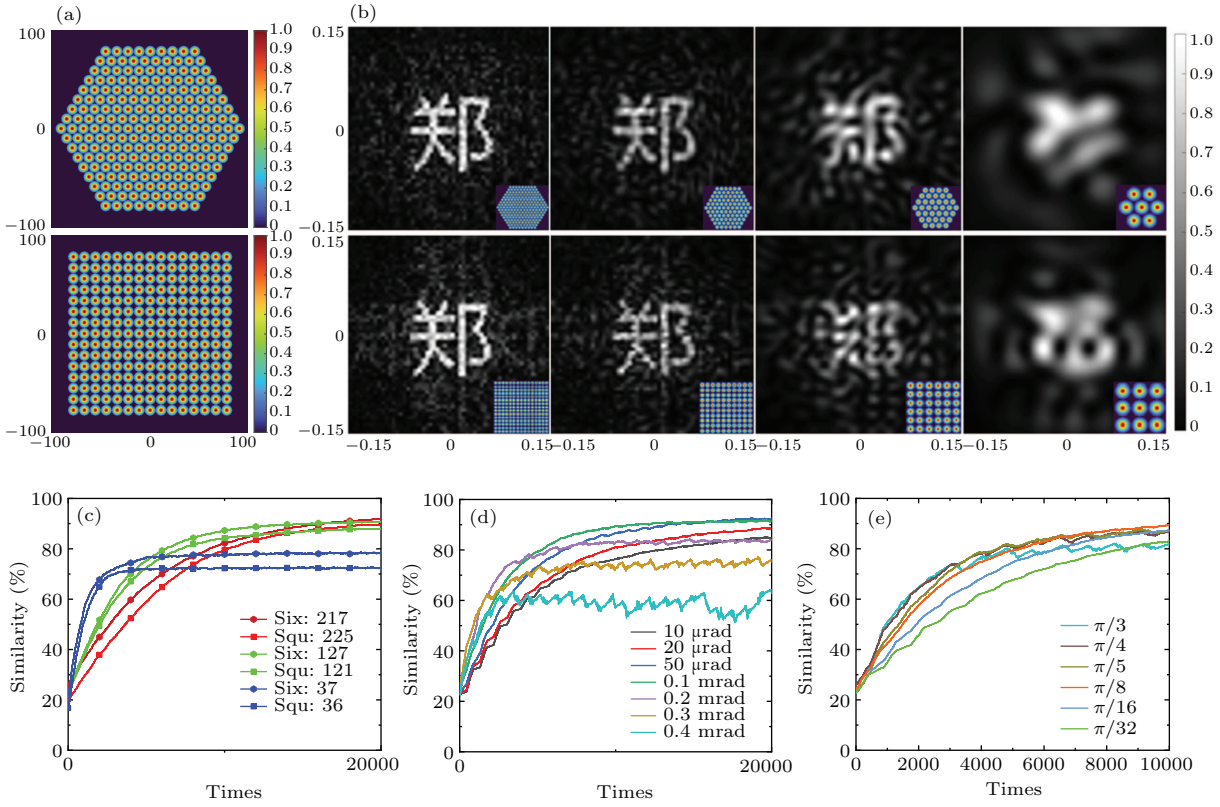


Fig. 3. (a) A hexagonal dense array consisting of 217 laser beams at the top and a square distributed beam array consisting of 225 laser beams at the bottom. (b) Convergence results for different numbers of hexagonal dense beam arrays and square arrays. The grayscale plot shows the THz shaping results and the inset shows the laser array distribution. (c) Differences in convergence speed and convergence effect between the hexagonal dense array structure and square array structure. The Six and the Squ in the illustration represent the hexagonal dense array and the square array structures, respectively, and the following number represents the number of beams composing the array. (d) Effect of the directional perturbation step on the convergence process. (e) Effect of the phase perturbation step on the convergence process.

The THz shaping process was simulated for hexagonal dense arrays and square arrays with different numbers of beams, respectively, and the results are shown in Fig. 3(c). We found that the greater the number of beams composing the array, the better the final THz shaping effect, but the disadvantage is that with increasing beam numbers composing the array, the convergence speed slows down.

At the same time, we chose 127 laser beams arranged in a hexagonal dense array to explore the influence of the optical axis orientation perturbation step size and phase perturbation step size on the convergence process using the same convergence algorithm. Among these, the optical axis orientation

disturbance includes horizontal disturbance and vertical disturbance. As shown in Figs. 3(d) and 3(e), we find that, regardless of the type of perturbation, a larger perturbation step size gives a greater advantage in the early stages of convergence but ultimately does not give the best convergence. Although the convergence speed of a small perturbation step is slow, it can converge stably and obtain the best convergence effect.

Next, we further adjusted the convergence strategy. Before that, each time we only adjusted the perturbation of one parameter of a beam and the convergence curve is shown as the orange curve (SC, serial control) in Fig. 4. This serial control method is inefficient, but it can achieve the effect of stable convergence. We have successively tried an overall parallel strategy in which each time a random perturbation is applied to all adjustable parameters of all beams. The convergence curve is shown as the yellow curve (FPC, full parallel control) in Fig. 4. We find that this method cannot converge completely and usually falls into the trap of a local extremum. Subsequently, we gradually reduced the number of parallel control parameters. We selected different numbers of beams for perturbation control in the total beam array N. For example, the purple curve (PC 50) in Fig. 4 represents the convergence curve for parallel control of all control parameters of 50 beams. The green curve (PC 25) represents that of 25 beams and the blue curve (PC 1) represents that of one beam. We found that the convergence rate slows down with the decrease in the number of beams and the final shaping effect continues to improve.

As shown above, based on the effects of perturbation step size, number of beams and array distribution on the convergence process, we subsequently adjusted the convergence strategy and adopted a dynamic optimization strategy. At the early stage of convergence, large perturbation step sizes for the optical axis and phase as well as multiple parallel control can be used to quickly achieve initial convergence. During the convergence process, the perturbation step sizes and the number of parallel channels are continuously adjusted according to the convergence state. At the late stage, smaller perturbation step sizes and single channel control are used to obtain the best shaping effect. As shown in Fig. 4, the red curve (OS) represents the convergence curve with the dynamic optimization strategy. The results demonstrate that the best convergence effect and the fastest convergence speed can be obtained simultaneously by reasonably adjusting the control strategy.

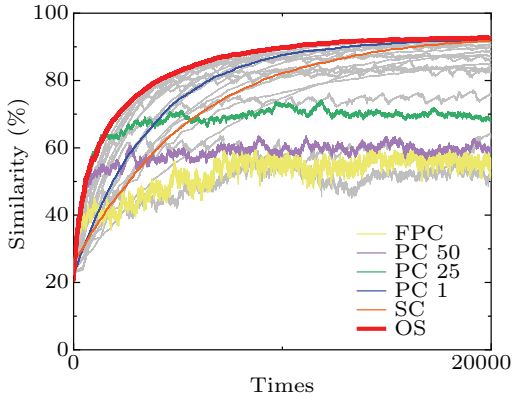


Fig. 4. Convergence curves for different strategies (FPC, full parallel control; PC, parallel control, with random selection of the number of beams for parallel control; SC, serial control; OS, dynamic optimization strategy). The gray curves are the convergence curves of other static convergence strategies.

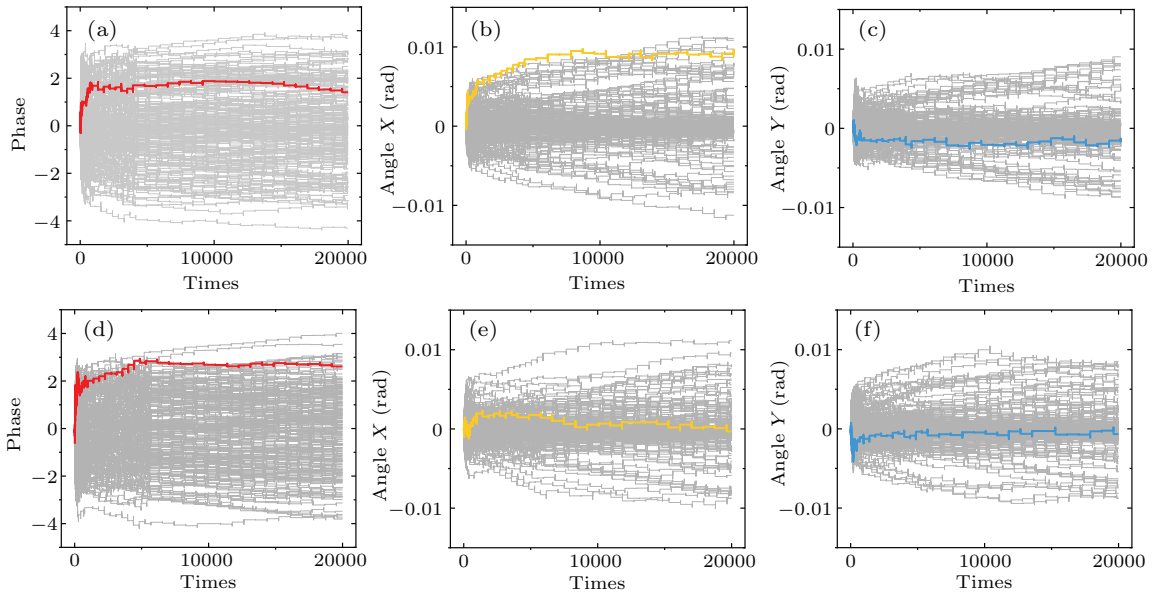


Fig. 5. Images of change in phase and beam deflection angle in convergence for two identical simulations: (a) image of phase change for the first convergence; (b) image of X-direction deflection angle change for the first convergence; (c) image of X-direction deflection angle change for the first convergence; (d) image of phase change for the second convergence; (e) image of X-direction deflection angle change for the second convergence; (f) image of X-direction deflection angle change for the second convergence. The colored and bold curves in each image are the phase and beam deflection angle change curves of a randomly selected beam from the 217-beam hexagonal dense array.

With the optimization algorithm, we performed simulations for the same target matrix for an array of 217 hexagonal dense arrays twice, and the final similarity was over 90%, with the change in phase and beam deflection angle shown in Fig. 5. Looking closely at these images we have randomly selected any channel in the laser array and highlighted the phase and beam deflection angle variation curves corresponding to two iterations of that channel, as shown in Figs. 5(a)–5(c) and 5(d)–5(f), respectively. It can be seen that the frequency and intensity of the jitter decreases as the number of iterations increases. The reason for this phenomenon is that the optimization algorithm can adjust the number of parallel channels and the step size according to the convergence state, from multiple parallel channels with large step size in the early stage to single serial channels with small step size in the later stage, ensuring that the model can achieve fast convergence in the early stage and the best convergence in the later stage. Furthermore, we found that although the same convergence was achieved twice, by observing the changes in phase and beam deflection angle of the randomly selected beam we found that the change paths and final states before and after the two convergences were completely different. Therefore, we can judge that the convergence process is random and the problem is actually a multi-solution problem.

The discussion on the convergence strategy will not stop here. We will try to use intelligent methods such as deep reinforcement learning in subsequent studies, and try to obtain more intelligent convergence methods.

The simulation was carried out using a hexagonal dense array of 217 laser beams for different objective functions by means of an optimization algorithm. As shown in Fig. 6(a), we have tried Chinese characters, Gaussian distribution and hollow beams with different apertures. As shown in Fig. 6(b), the similarity between the convergence result and the target is more than 90%, and they are all successful. These attempts further illustrate the universality of this method and have great application prospects in scientific research and production processes.

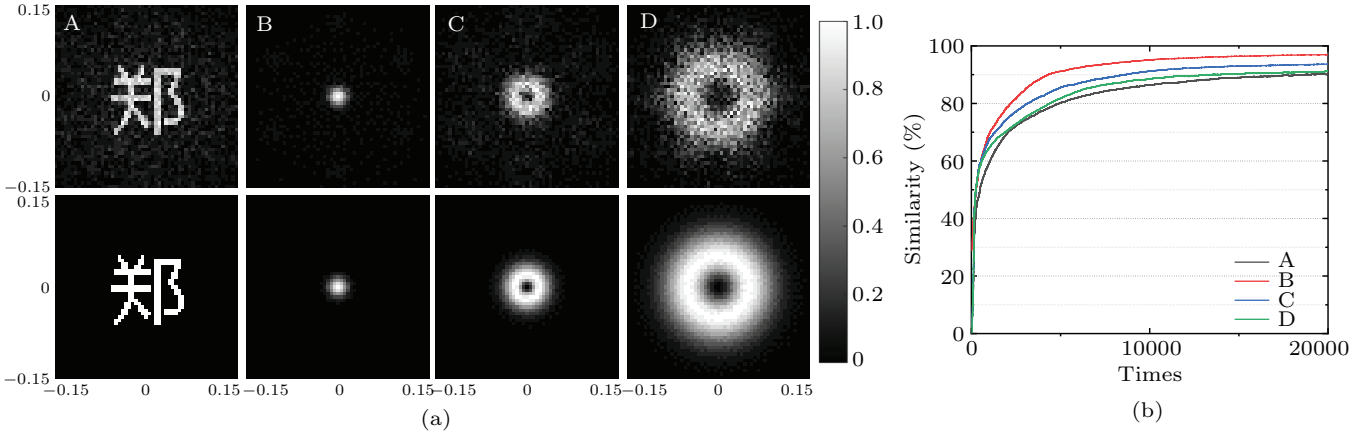


Fig. 6. (a) Comparison of convergence results with the target distribution. The first row is the convergence result and the second row is the target distribution. (b) Convergence curves for Fig. 6(a).

This method not only achieves THz shaping but also finds the beam patterns with higher energy conversion efficiency and breaks the energy limit of THz waves at high power. As the energy of a single laser pulse increases, the intensity of the THz yield tends to encounter an upper limit.[18] The upper limit is mainly due to the absorption and shielding of THz waves by the plasma. The higher the laser single pulse energy that is used, the higher the electron density of the excited air plasma and the higher the plasma frequency that is obtained. Eventually, the THz waves in the high electron density region in the plasma are completely absorbed and shielded, and the effective plasma that actually generates the THz waves does not increase with increase in the single pulse energy. Therefore, we can divide the laser-excited air plasma into two categories. One is the effective plasma that can generate THz waves. The other is the ineffective plasma that has a strong absorption and shielding effect on THz waves. The enhanced laser-to-THz wave conversion efficiency by using long-focus lens focusing[28] and special beams[7] is in fact an increase in conversion efficiency that can be reached by increasing the number of effective plasmas, which can be evaluated using the number or volume of plasma electrons. In this way, our pursuit of the energy conversion efficiency of THz radiation can be converted into pursuit of the increase in the effective plasma quantity. CBC technology is an excellent solution to this problem. In fact, the system could be directed toward getting stronger THz wave energy simply by changing the evaluation function of the system, for example using the power in the barrel as the evaluation function.

4. Conclusion and perspectives

Generally, the THz radiation generated by traditional Gaussian laser beams has a hollow distribution due to coherence and plasma absorption, which is not conducive to

the propagation and application of THz waves. THz shaping technology based on laser coherent synthesis enables the advantages of 'air method' THz wave sources to be fully exploited. It can directly complete THz shaping by controlling the plasma electron density distribution and flexibly adjust the THz distribution according to the actual demands.

Compared with traditional methods, the use of laser CBC technology can not only achieve modulation of the excited plasma through the modulation of the laser field, and thus achieve THz shaping, but can also further break the upper limit of the energy conversion rate from high-power laser to THz wave. It can also achieve THz mode modulation by reproducing certain plasmas with a special distribution state to excite THz radiation with a desirable distribution. At the algorithmic level, we pioneered the application of the two-dimensional correlation coefficient function as an evaluation function to the SPGD iterative algorithm. Compared with methods such as the mean square difference method, this method does not easily fall into local extremes and converges quickly. In summary, this technology bridges the gap in the field of high-intensity THz generation and beam shaping technology. It is also expected that the physical mechanism of THz generation in plasma through this technology will be further investigated to obtain THz sources with a better quality; this will be very valuable for scientific research and practical application.

Acknowledgements

Project supported by the National Natural Science Foundation of China (Grant Nos. 12074272 and 61905271), the National Defense Science and Technology Innovation Special Zone Project of China (Grant No. 20-163-02-ZT-008-009-01) and Guangdong Basic and Applied Basic Research Foundation (Grant No. 2020A1515011083).

References

[1] Cook D J and Hochstrasser R M 2000 *Opt. Lett.* **25** 1210
[2] Kress M, Löffler T, Eden S, Thomson M and Roskos H G 2004 *Opt. Lett.* **29** 1120
[3] Zhong H, Karpowicz N and Zhang X C 2006 *Appl. Phys. Lett.* **88** 261103
[4] Clerici M, Peccianti M, Schmidt B, Caspani L, Shalaby M, Giguére M, Lotti A, Couairon A, Légaré F, Ozaki T, Faccio D and Morandotti R 2013 *Phys. Rev Lett.* **110** 253901
[5] Chen Y P, Yamaguchi M, Wang M C and Zhang X C 2007 *Appl. Phys. Lett.* **91** 251116
[6] Kumar S, Vij S, Kant N, Mehta A and Thakur V 2021 *Eur. Phys. J. Plus* **136** 1
[7] Liu K, Koulouklidis A D, Papazoglou D G, Tzortzakis S and Zhang X C 2016 *Optica* **3** 605
[8] Zhang Z L, Zhang J Y, Chen Y P, Xia T H, Wang L Z, Han B N, He F, Sheng Z and Zhang J 2022 *Ultrafast Science* **2022** 9870325
[9] Zhou P, Liu Z J, Wang X L, Ma Y X, Ma H T, Xu X J and Guo S F 2009 *IEEE J. Sel. Top. Quant.* **15** 248
[10] Thomas M S 2006 *Opt. Express* **14** 12188
[11] Vorontsov M A and Lachinova S L 2008 *J. Opt. Soc. Am. A* **25** 1949
[12] Hou T Y, Y An, Chang Q, Ma P, Li J, Huang L J, Dong Z, Jian W, Su R, Ma Y X and P Zhou 2020 *Photon. Res.* **8** 715
[13] Chavez C S, Padgett M J, Allison I, New G H C, Gutierrez V J C, Neil A T O, Vicar I M and Courtial J 2002 *J Opt. B-Quantum S O* **4** S52
[14] Genevet P, Lin J, Kats M A and Capasso F 2012 *Nat. Commun.* **3** 1278
[15] Mohammadi S M, Daldorff L K S, Bergman J E S, Karlsson R L, Thidé B, Forozesh K, Carozzi T D and Isham B 2010 *IEEE Trans. Antennas Propag.* **58** 565
[16] Thide B, Then H, SjoHolm J, Palmer K, Bergman J, Carozzi T D, Istomin Y N, Ibragimov N H and Khamitova R 2007 *Phys. Rev. Lett.* **99** 087701
[17] Li X N, Zhou L and Zhao G Z 2019 *Acta Phys. Sin.* **68** 238101 (in Chinese)
[18] Kim K Y, Taylor A J, Glownia J H and Rodriguez G 2008 *Nat. Photonics* **2** 605
[19] Fan T Y 2005 *IEEE J. Sel. Top. Quant.* **11** 567
[20] Lombard L, Azarian A, Cadoret K, Bourdon P, Goular D, Canat G, Jolivet V, Jaouën Y and Vasseur O 2011 *Opt. Lett.* **36** 523
[21] Daniault L, Hanna M, Lombard L, Zaouter Y, Mottay E, Goular D, Bourdon P, Druon F and Georges P 2011 *Opt. Lett.* **36** 621
[22] Chanteloup J C, Bellanger S, Daniault L, Fsaifes I, Veinhard M, Bourderionnet J, Larat C, Lallier E and Brignon A 2021 *Proc. SPIE, Fiber Lasers XVIII: Technology and Systems*, 116651H
[23] Kim K Y, Glownia J H, Taylor A J and Rodriguez G 2007 *Opt. Express* **15** 4577
[24] You Y S, Oh T I and Kim K Y 2012 *Phys. Rev. Lett.* **109** 183902
[25] Gorodetsky A, Koulouklidis A D, Massaouti M and Tzortzakis S 2014 *Phys. Rev. A* **89** 033838
[26] Keldysh L V 1965 *Sov. Phys. JETP* **20** 1307
[27] Perelomov A, Valentin S P and Terentev M V 1966 *Sov. Phys. JETP* **23** 924
[28] Amico C D, Houard A, Akturk S, Liu Y, Bloas J L, Franco M, Prade B, Couairon A, Tikhonchuk V T and Mysyrowicz A 2008 *New J. Phys.* **10** 013015